

Finite Element Analysis

Alex Carey

December 20, 2025

1 Poisson Equation

System Setup

The Poisson system is defined by the following partial differential equation 1 with f defined on the domain Ω in 2 and boundary conditions defined on the boundary $\partial\Omega$ in 3.

$$-\nabla^2 u = f \quad \text{in } \Omega \quad (1)$$

$$f(x, y) = 2\pi^2 \sin(\pi x) \cos(\pi y) \quad (2)$$

$$u(0, y) = u(1, y) = 0, \quad \partial_y u(x, y)|_{y=0} = \partial_y u(x, y)|_{y=1} = 0 \quad (3)$$

the system admits the exact solution $u(x, y) = \sin(\pi x) \cos(\pi y)$ which we verify by substitution into 1.

$$-\nabla^2(\sin(\pi x) \cos(\pi y)) = 2\pi^2 \sin(\pi x) \cos(\pi y) = f(x, y) \quad (4)$$

and further we consider the derivative with respect to y given $\partial_y u(x, y) = -\sin(\pi x) \sin(\pi y)$ which is zero at $y = 0$ and $y = 1$ as required by Neumann boundary condition. The Dirichlet boundary condition is also clearly satisfied.

Question 1

The Ritz-Galerkin principle states that the solution to the Poisson Equation is equivalent to the minimiser of the function defined

$$I[u] = \int_{\Omega} \left(\frac{1}{2} |\nabla u|^2 - fu \right) d\Omega. \quad (5)$$

To find this minimiser we consider the variation of $I[u]$ with respect to some variational function δu such that $u \rightarrow u + \delta u$ is considered. To maintain the boundary conditions for this new function we require that $\delta u = 0$ on the Dirichlet boundary and $\partial_y \delta u = 0$ on the Neumann boundary. We consider the variation in some limit $\epsilon \rightarrow 0$ such that

$$\frac{dI}{d\epsilon} = \int_{\Omega} \left(\frac{1}{2} \nabla u \cdot \nabla \delta u - f \delta u \right) d\Omega. \quad (6)$$

If u is the minimiser of I then this variation must be zero for all possible δu which gives us the weak form of the Poisson equation. We have that u is a solution to the Poisson system if u satisfies

$$\int_{\Omega} \nabla u \cdot \nabla \delta u \, d\Omega = \int_{\Omega} f \delta u \, d\Omega \quad \forall \delta u \quad (7)$$

where δu satisfies the altered boundary conditions described above.

The test function v that is used in the weak form is equivalent to the variational function δu as both functions are arbitrary and satisfy the same boundary conditions.

Question 2

We introduce the finite element basis functions $\Phi = \{\phi_i : i = 1, \dots, N\}$ defined on the domain Ω such that we can approximate the solution

$$u \approx u_h = \sum_{j=1}^N u_j \phi_j \quad (8)$$

where u_j are the coefficients of the basis functions and N is the number of basis functions. We also consider the set of test functions to be equivalent to the set of basis functions such that $v = \phi_i$ for some $i = 1, \dots, N$. As the basis functions span the solution space and are linearly independent, we only require that the weak form is satisfied for each basis function.

Substituting u_h into the Ritz-Galerkin formulation gives us

$$J[u_h] = \int_{\Omega} \left(\frac{1}{2} |\nabla u_h|^2 - f u_h \right) d\Omega. \quad (9)$$

where we aim to find the minimal coefficients u_j . We define the tensors \mathbf{M} and \mathbf{b} as follows

$$M_{ij} = \int_{\Omega} \nabla \phi_i \cdot \nabla \phi_j \, d\Omega \quad (10)$$

$$b_i = \int_{\Omega} f \phi_i \, d\Omega \quad (11)$$

such that the functional can be expressed as

$$J[\mathbf{u}] = \frac{1}{2} \mathbf{u}^T \mathbf{M} \mathbf{u} - \mathbf{u}^T \mathbf{b} \quad (12)$$

where $\mathbf{u} = [u_1, u_2, \dots, u_N]^T$ is the vector of coefficients.

We consider also the substitution into the weak formulation giving

$$\int_{\Omega} \nabla \left(\sum_{j=1}^N u_j \phi_j \right) \cdot \nabla \phi_i \, d\Omega = \int_{\Omega} f \phi_i \, d\Omega \quad \forall i = 1, \dots, N. \quad (13)$$

where we apply the same matrix operators to express this as

$$\mathbf{M} \mathbf{u} = \mathbf{b}. \quad (14)$$

We see that these two results are equivalent when we consider the minimisation of 12 with respect to \mathbf{u} giving

$$\frac{dJ}{d\mathbf{u}} = \mathbf{Mu} - \mathbf{b} = 0 \quad (15)$$

recovering the weak form expression.

Question 3

We consider a quadrilateral mesh with the set of elements given by the tessellation of the domain

$$\Omega = \bigcup_{k=1}^{N_K} K_k \quad (16)$$

for $k = 1, \dots, N_K$ where K represent disjoint subsets of Ω such that each is described by four nodes at the corners of the quadrilateral which we label $0, \dots, 3$ in a counter-clockwise manner starting from the bottom left corner.

We define a reference element $\hat{K} = [-1, 1] \times [-1, 1]$ with local coordinates (\hat{x}, \hat{y}) and define the map from the reference element onto a physical element K by some function $\mathbf{F}_K : \hat{K} \rightarrow K$ such that

$$\mathbf{x} = \mathbf{F}_K(\hat{x}, \hat{y}) = \sum_{\alpha=0}^3 \mathbf{x}_{\alpha,k} \hat{\phi}_\alpha(\hat{x}, \hat{y}) \quad (17)$$

for some shape functions $\hat{\phi}_\alpha : \hat{K} \rightarrow [0, 1]$ defined on the element K_k . In the quadrilateral case we have four shape functions defined as follows

$$\hat{\phi}_0(\hat{x}, \hat{y}) = \frac{1}{4}(1 - \hat{x})(1 - \hat{y}) \quad (18)$$

$$\hat{\phi}_1(\hat{x}, \hat{y}) = \frac{1}{4}(1 + \hat{x})(1 - \hat{y}) \quad (19)$$

$$\hat{\phi}_2(\hat{x}, \hat{y}) = \frac{1}{4}(1 + \hat{x})(1 + \hat{y}) \quad (20)$$

$$\hat{\phi}_3(\hat{x}, \hat{y}) = \frac{1}{4}(1 - \hat{x})(1 + \hat{y}) \quad (21)$$

where \mathbf{x}_α are the physical coordinates of the nodes of element K .

The resulting Jacobian of this transformation is given

$$\mathbf{J}_K(\hat{x}, \hat{y}) = \begin{bmatrix} (1 - \hat{y})(x_{1,k} - x_{0,k}) + (1 + \hat{y})(x_{2,k} - x_{3,k}) & (1 - \hat{y})(y_{1,k} - y_{0,k}) + (1 + \hat{y})(y_{2,k} - y_{3,k}) \\ (1 - \hat{x})(x_{3,k} - x_{0,k}) + (1 + \hat{x})(x_{2,k} - x_{1,k}) & (1 - \hat{x})(y_{3,k} - y_{0,k}) + (1 + \hat{x})(y_{2,k} - y_{1,k}) \end{bmatrix} \quad (22)$$

where $(x_{\alpha,k}, y_{\alpha,k})$ are the physical coordinates of node α of element K_k .

We can then reform the matrix system from Question 2 in terms of the reference elements with the key substitution

$$\int_{K_k} g(x, y) dK = \int_{\hat{K}} g(\mathbf{F}_K) |\det(\mathbf{J}_K)| d\hat{K} \quad (23)$$

yielding the matrix entries

$$M_{ij} = \sum_{k=1}^{N_K} \int_{\hat{K}} \nabla \phi_i(\mathbf{F}_K) \cdot \nabla \phi_j(\mathbf{F}_K) |\det(\mathbf{J}_K)| d\hat{K} \quad (24)$$

$$b_i = \sum_{k=1}^{N_K} \int_{\hat{K}} f(\mathbf{F}_K) \phi_i(\mathbf{F}_K) |\det(\mathbf{J}_K)| d\hat{K} \quad (25)$$

In the case of the matrix \mathbf{M} we further consider the gradient terms which require the inverse of the Jacobian such that $\nabla \phi_i(\mathbf{F}_K) = \mathbf{J}_K^{-1} \hat{\nabla} \hat{\phi}_i$ where $\hat{\nabla}$ is the gradient operator with respect to the reference coordinates. This gives us the final form

$$M_{ij} = \sum_{k=1}^{N_K} \int_{\hat{K}} \left(\mathbf{J}_K^{-1} \hat{\nabla} \hat{\phi}_i \right) \cdot \left(\mathbf{J}_K^{-1} \hat{\nabla} \hat{\phi}_j \right) |\det(\mathbf{J}_K)| d\hat{K} \quad (26)$$

1.1 Code Output

A numerical implementation was created in python with the following outputs. The following figures show the output for u_h computed in Figure 1. The differences to the exact solution appear as in Figures 2, 3 and 4 for grid sizes of 128, 64 and 16 respectively.

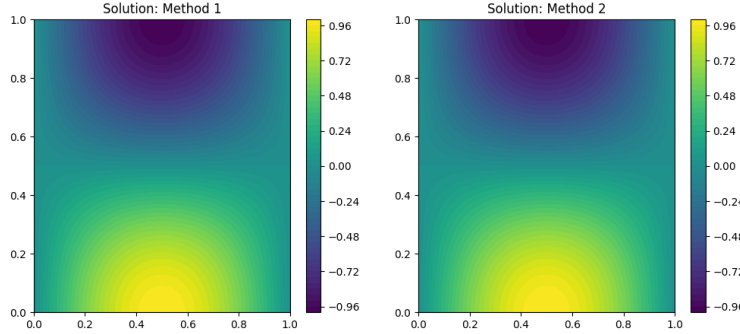


Figure 1: Finite Element Solution u_h to the Poisson Equation with a grid size of 128 and polynomials of order 1.

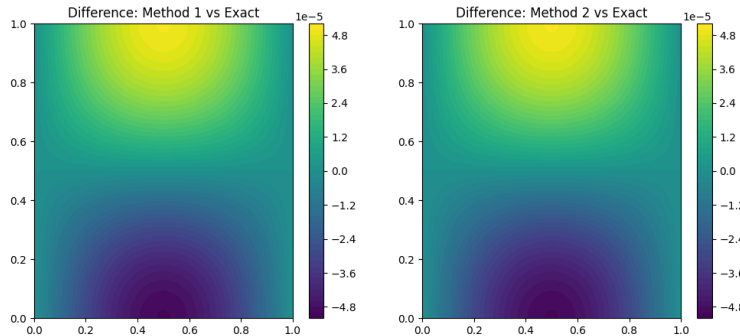


Figure 2: Error $u - u_h$ between the finite element solution and exact solution for a grid size of 128 and polynomials of order 1.

We have the L2 Errors for a number of different mesh sizes and polynomial orders as seen in Figure 5. We observe the order 1 convergence rate for the linear elements, order 2 for the quadratic elements and a

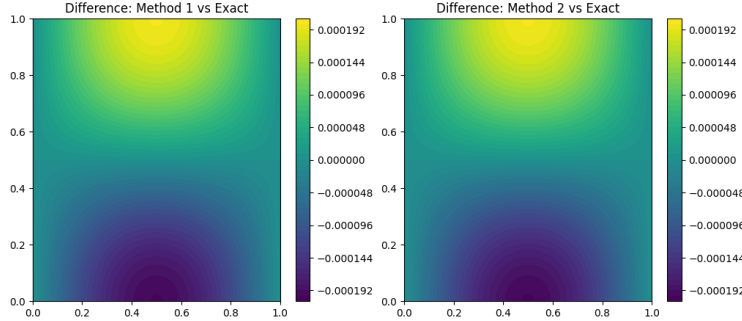


Figure 3: Error $u - u_h$ between the finite element solution and exact solution for a grid size of 64 and polynomials of order 1.

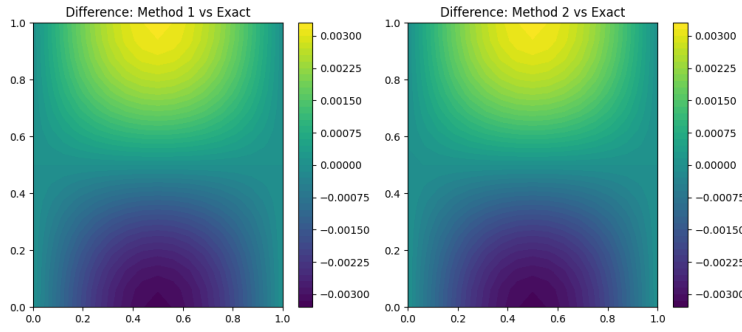


Figure 4: Error $u - u_h$ between the finite element solution and exact solution for a grid size of 16 and polynomials of order 1.

slightly higher order for the cubic elements. Note that this behaviour begins to degenerate for the higher orders as the round-off errors begin to dominate for large numbers of elements and high polynomial orders where more operations are required.

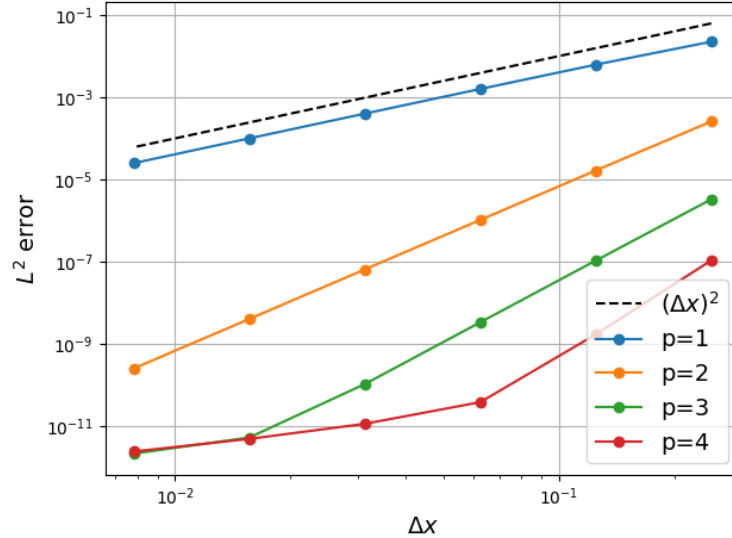


Figure 5: L2 Error convergence for different mesh sizes and polynomial orders.

For the alternate system formulation with the exact solution given

$$u(x, y) = \sin(5\pi x)y^2(2y - 3) \quad (27)$$

and the corresponding $f(x, y)$ defined by

$$f(x, y) = -(-\pi^2 y^2(2y - 3) + 6(2y - 1)) \sin(5\pi x) \quad (28)$$

we observe the following solution and the error

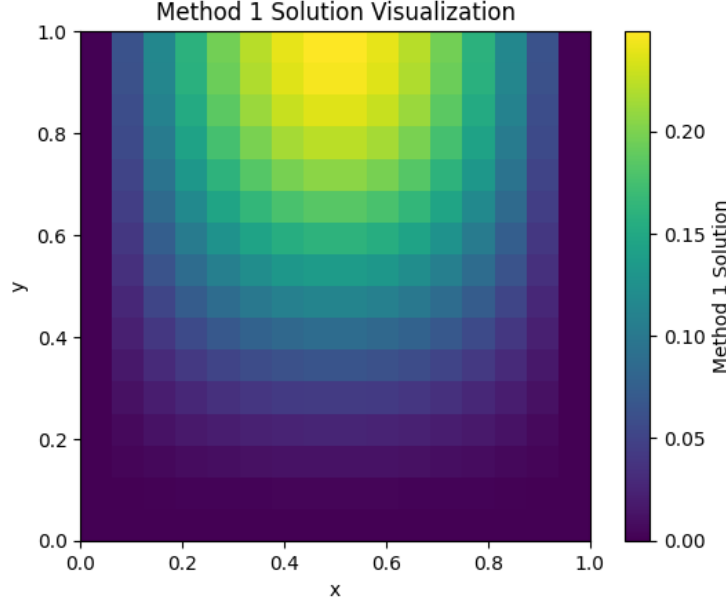


Figure 6: Finite Element Solution u_h to the alternate Poisson Equation .

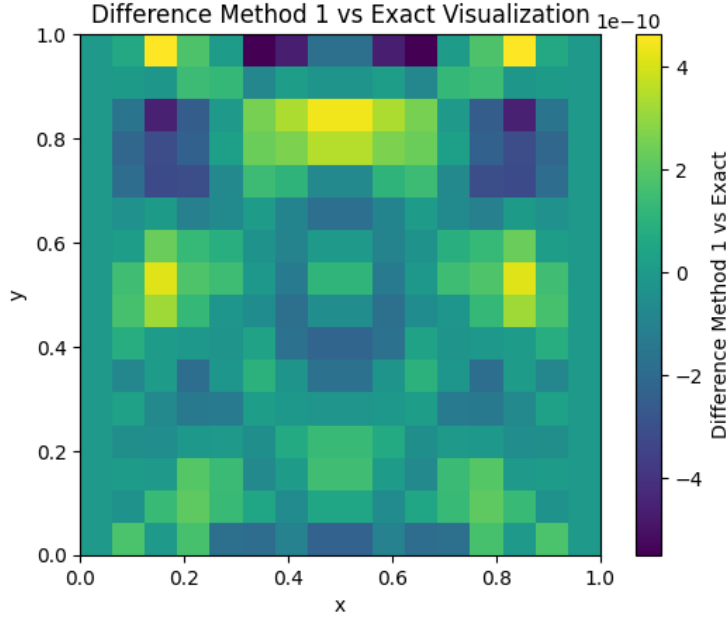


Figure 7: Error $u - u_h$ between the finite element solution and exact solution .

2 Groundwater and Canal Flow

System Setup

We consider the groundwater flow system defined by the following PDE with boundary conditions and ODE.

$$\partial_t(w_v h_m) - \alpha g \partial_y(w_v h_m \partial_y h_m) = w_v \frac{R}{m_{\text{por}} \sigma_e}, \quad y \in [0, L_y], \quad (29)$$

$$\partial_y h_m = 0 \quad \text{at } y = L_y, \quad (30)$$

$$h_m(0, t) = h_{cm}(t) \quad \text{at } y = 0, \quad (31)$$

$$L_c w_v \frac{dh_{cm}}{dt} = w_v \frac{m_{\text{por}}}{2} \sigma_e \alpha g \partial_y(h_m^2) |_{y=0} - w_v \sqrt{g} \max\left(\frac{2}{3} h_{cm}(t), 0\right)^{3/2}. \quad (32)$$

for a groundwater system of in the region $[0, L_y]$ connected to a canal between $y = 0$ and $y = L_c$ where the height of the water is $h_m(y, t)$ in the groundwater and $h_{cm}(t)$ in the canal. The outflow flux from the canal is governed by a weir equation resulting in the equations above.

Question 1

We define the finite element basis function

$$\Psi = \{\phi_i : \phi_i \in C^0[0, L_y], \phi_i|_K \in \mathbf{P}_1(K)\} \quad (33)$$

for all elements K in the mesh of $[0, L_y]$ where $\mathbf{P}_1(K)$ is the space of linear polynomials on the element K . We approximate the solution as

$$h_m(y, t) \approx h_m^h(y, t) = \sum_{j=1}^N h_j(t) \phi_j(y) \quad (34)$$

where $h_j(t)$ are the time-dependent coefficients of the basis functions and N is the number of basis functions. We also consider the set of test functions to be equivalent to the set of basis functions such that $v = \phi_i$ for some $i = 1, \dots, N$.

We define some test function $v(y, t)$ and multiply the PDE by this function to given

$$\int_0^{L_y} \partial_t(h_m^h)v dy - \int_0^{L_y} \alpha g \partial_y(h_m^h \partial_y h_m^h)v dy = \int_0^{L_y} \frac{R}{m_{\text{por}}\sigma_e} v dy. \quad (35)$$

For ease we define $F = \frac{1}{2}\alpha g \partial_y(h_m^h)^2$ and integration by parts gives

$$\int_0^{L_y} \partial_t(h_m^h)v dy = [Fv]_0^{L_y} - \int_0^{L_y} F \partial_y v dy + \int_0^{L_y} \frac{R}{m_{\text{por}}\sigma_e} v dy. \quad (36)$$

where Fv is representative of the flux into the canal. The Neumann boundary condition at $y = L_y$ gives $F(L_y) = 0$ and so we can eliminate the flux through this boundary by considering the ODE for the canal height. This results in the form

$$\int_0^{L_y} \partial_t(h_m^h)v dy + \frac{v_0 L_c \partial_t h_m(0, t)}{m_{\text{por}}\sigma_e} = - \int_0^{L_y} F \partial_y v + \frac{v R}{m_{\text{por}}\sigma_e} v dy - \frac{v_0 Q_c}{m_{\text{por}}\sigma_e} \quad (37)$$

where the discharge $Q_c(h_m(0, t)) = \sqrt{g} \max(\frac{2}{3}h_m(0, t), 0)^{3/2}$.

Application of the explicit Euler method for discretisation of the time derivative yields

$$\int_0^{L_y} h_m^{n+1} v dy + \frac{v_0 L_c h_m^{n+1}(0)}{m_{\text{por}}\sigma_e} = \int_0^{L_y} h_m^n v dy + \frac{v_0 L_c h_m^n(0)}{m_{\text{por}}\sigma_e} - \Delta t \left(\int_0^{L_y} F^n \partial_y v + \frac{v R^n}{m_{\text{por}}\sigma_e} v dy - \frac{v_0 Q_c^n}{m_{\text{por}}\sigma_e} \right) \quad (38)$$

We define the tensors as follows

$$M_{ij} = \int_0^{L_y} \phi_i \phi_j dy \quad (39)$$

$$b_i^n = - \int_0^{L_y} \alpha g h_m^n \partial_y \phi_i + \frac{R^n}{m_{\text{por}}\sigma_e} \phi_i dy \quad (40)$$

such that the scheme can be expressed in matrix form as

$$M_{ij} h_j^{n+1} + \frac{\delta_{i1} L_c}{m_{\text{por}}\sigma_e} h_m^{n+1}(0) = M_{ij} h_j^n + \frac{\delta_{i1} L_c}{m_{\text{por}}\sigma_e} h_m^n(0) + \Delta t \left(b_i^n - \frac{v_0 Q_c^n}{m_{\text{por}}\sigma_e} \right) \quad (41)$$

where we have used the Kronecker delta δ_{i1} to select the test function at the boundary $y = 0$ (all other test functions are zero at this point).

Code Output

$\theta = 0$, **P₁(Linear Elements)**

A constant rainfall case with a fully explicit scheme on linear elements.

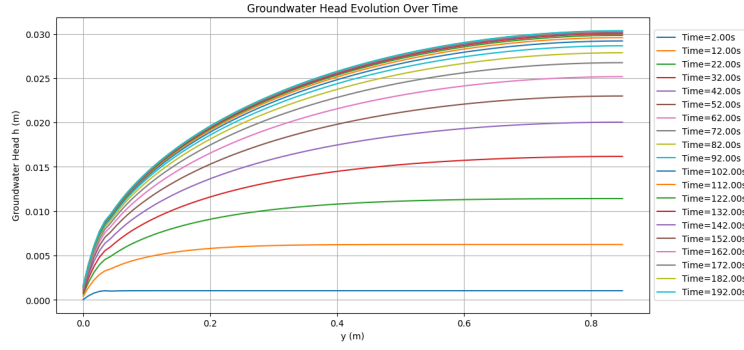


Figure 8: Plot of the groundwater height h_m at various times.

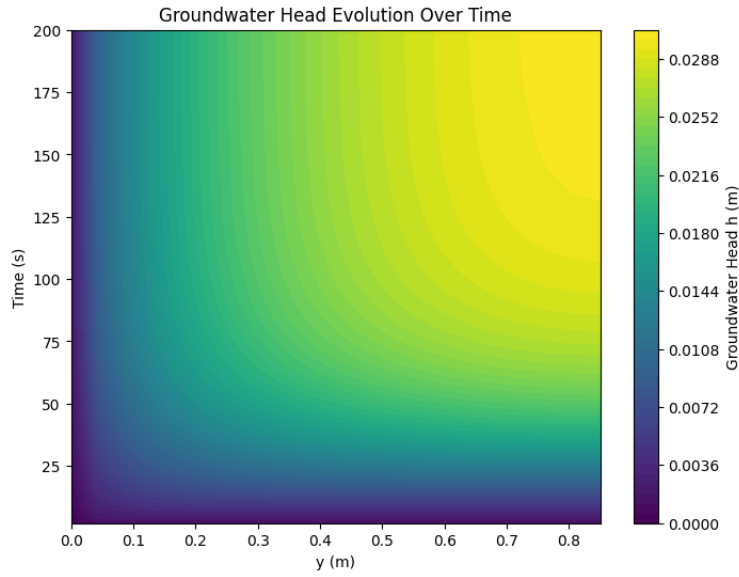


Figure 9: Contour plot of the groundwater height h_m over time.

$\theta = 0.5, \mathbf{P}_2(\text{Quadratic Elements})$

A constant rainfall case with a Crank-Nicolson scheme on quadratic elements.

Variable Rainfall: $\theta = 0.5, \mathbf{P}_2(\text{Quadratic Elements})$

A variable rainfall case with a Crank-Nicolson scheme on quadratic elements.

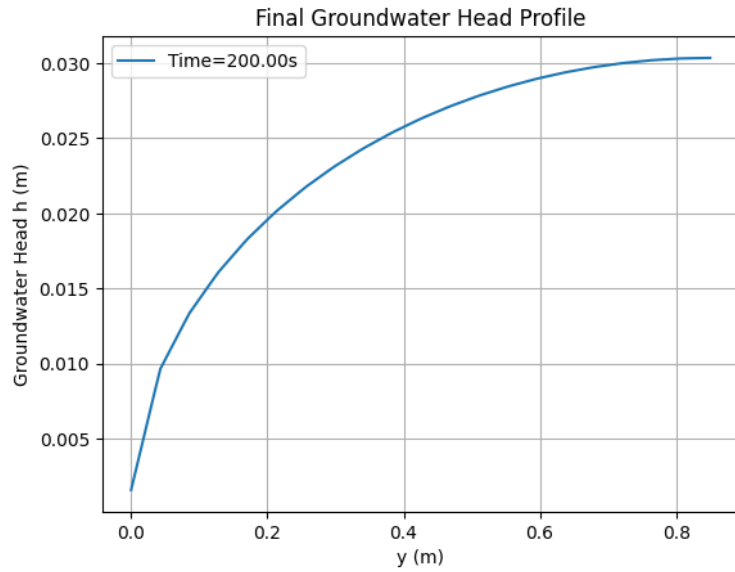


Figure 10: Plot of the final (steady) groundwater profile..

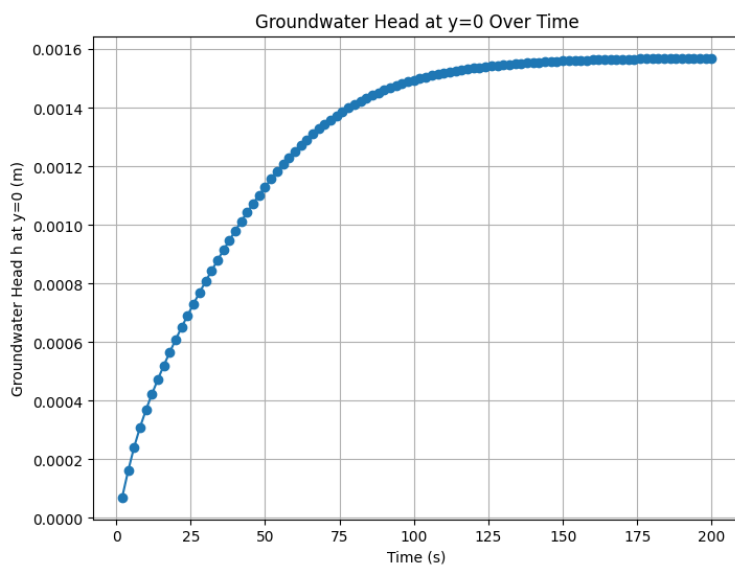


Figure 11: Plot of the canal height h_{cm} over time.

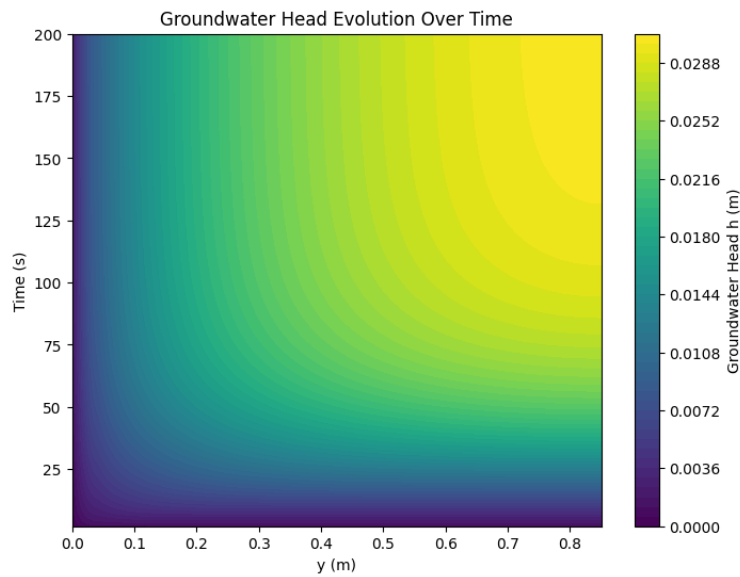


Figure 12: Contour plot of the groundwater height h_m over time.

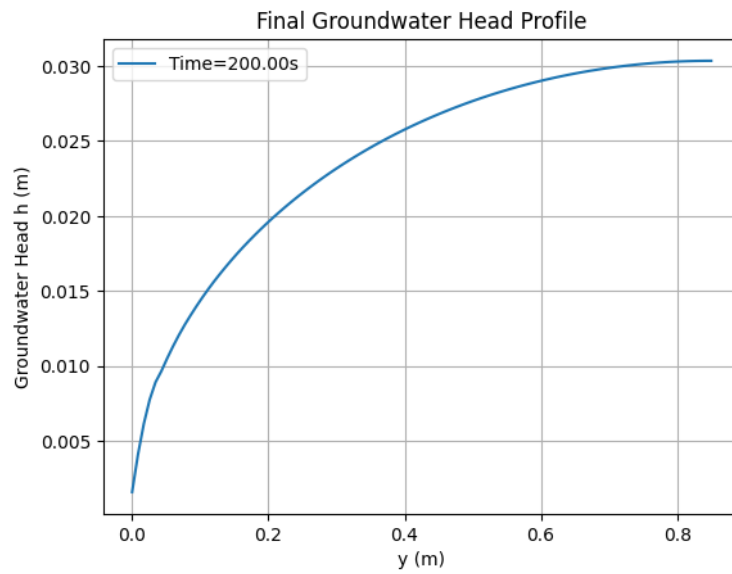


Figure 13: Plot of the final (steady) groundwater profile..

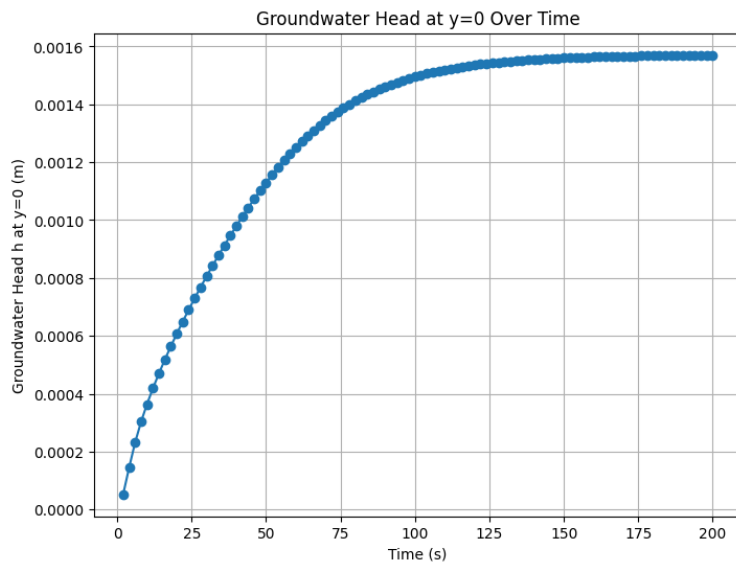


Figure 14: Plot of the canal height h_{cm} over time.

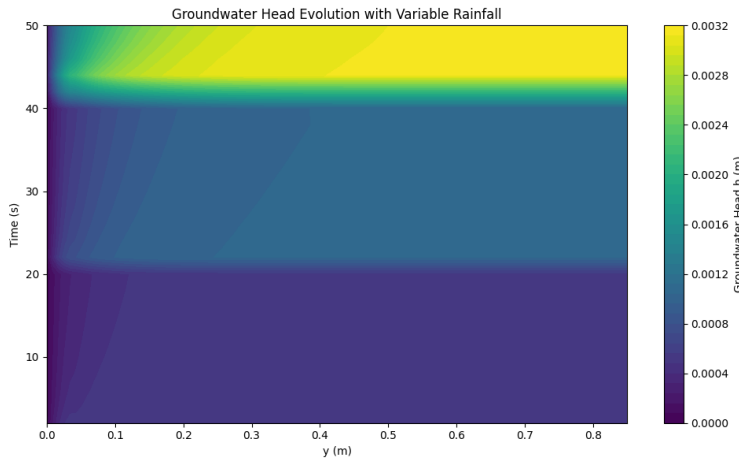


Figure 15: Contour plot of the groundwater height h_m over time.

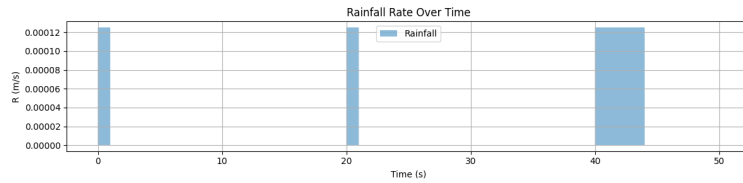


Figure 16: Plot of the activation of rainfall over time.

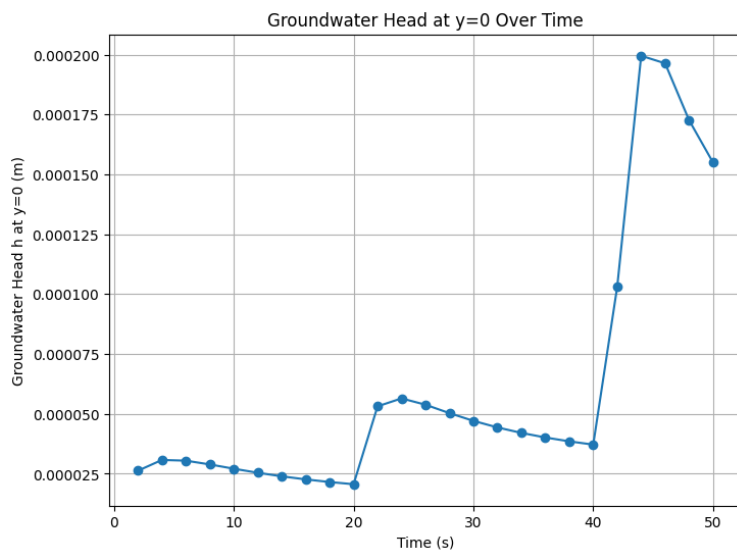


Figure 17: Plot of the canal height h_{cm} over time.